Maskless lithography

Article *in* Materials Today · February 2005

DOI: 10.1016/S1369-7021(05)00699-1

4 authors, including:

Dario Gil
IBM
31 PUBLICATIONS **801** CITATIONS

SEE PROFILE

Maskless lithography

by Rajesh Menon, Amil Patel, Dario Gil[†], and Henry I. Smith*

The increasingly important role of maskless lithography in industry, research, and emerging applications in nanoscale science and engineering is discussed. The various forms of maskless lithography are reviewed with major emphasis on zone-plate-array lithography, a new paradigm that promises low cost and extendibility to the limits of the lithographic process.

The information revolution, which has dramatically altered world economies and our everyday lives via personal computers, e-mail, the Internet, and wireless communication, is based upon integrated electronics. Low-cost Si chips containing hundreds of millions of transistors are made using a technology we call lithography. Lithography puts spatial information into a substrate, and it is this information that determines functionality. Lithography has been the key technology in the information revolution and will almost certainly underpin future technological revolutions based on nanotechnology.

The form of lithography used in the Si semiconductor industry is optical projection lithography (OPL). In this technique, a pattern is first created on a reticle or mask at four times the desired final size, and the image of the mask is projected onto a Si wafer by a large (over 1000 kg) and very expensive reduction lens. The rapid advances in the semiconductor industry have been enabled by advances in OPL technology and in the quality of the photoresist that records the projected image. Today, in semiconductor manufacturing, the operating wavelength in advanced OPL systems (so-called 'steppers' or 'scanners') is 193 nm, the throughput is 60 or more Si wafers per hour, the field size is about 20 mm x 30 mm, and the minimum feature size is ~90 nm. To achieve such results, a variety of resolution-enhancement techniques (RETs) are employed, including: phase-shift masks, off-axis illumination, and optical proximity-effect correction (OPC)[1,2]. In the near future, water-immersion optics will be used to further improve

Research Laboratory of Electronics,
Massachusetts Institute of Technology,
Cambridge, MA 02139, USA
Also, Lumarray, LLC
Cambridge, MA 02139, USA
*E-mail: hismith@nano.mit.edu

[†]Currently at IBM

ISSN:1369 7021 © Elsevier Ltd 2005

the resolution and depth-of-focus achievable with 193 nm OPL[3].

The crisis in lithography

Despite the impressive and rapid advances, and the extensive research being conducted in OPL, a crisis is apparent that takes many forms and has many implications. In the semiconductor industry, the crisis includes: the difficulty, cost, and delay associated with designing the OPC features for a mask; the cost and long delays in making the masks; and the uncertainties associated with future scaling of transistor dimensions. The cost of a set of masks for producing a chip can exceed $2 million, and yet in most cases only a few wafers will be produced. The difficulty, time, and cost associated with designing and repairing a mask leads chip designers to be conservative, which stifles innovation. Maskless optical lithography, as described in this paper, offers a path around many of these difficulties. For low volume production, i.e. when only a limited number of wafers is required, as in application-specific integrated circuits, a throughput of one to a few wafers per hour would be adequate. Maskless optical lithography could well represent a disruptive technology that changes the complexion and direction of the semiconductor industry.

Beyond the semiconductor industry, there is a wide range of applications that require high-quality lithography. To name a few: magnetic information storage, microphotonics, microelectromechanical systems, microfluidics, and nanotechnology. The latter, a field that is only beginning to take shape and will undoubtedly have a wide range of forms, will almost certainly require methods and systems of lithography that differ substantially from those used in the semiconductor industry. For nanotechnology, the cost of lithography must be lowered by a large factor over that encountered in the semiconductor industry. Moreover, when used for the finest geometries, the OPL tools of the semiconductor industry are configured to produce only the 'Manhattan' geometries required for transistors, not patterns of arbitrary geometry. For example, the RETs employed are generally not appropriate for producing ring-shaped patterns at the same resolution that they can produce fine isolated lines. The capital cost (~$20 million) and maintenance cost of semiconductor-industry OPL tools put them out of reach for researchers in nanoscale science and engineering. The cost and delays associated with masks stifle innovation here as well. Maskless optical lithography holds the promise of meeting the resolution, throughput, and other requirements of the semiconductor industry, as well as those of other, emerging applications.

Various forms of maskless lithography

The forms of maskless lithography include: scanning electron-beam lithography (SEBL), focused ion-beam (FIB) lithography, multiaxis electron-beam lithography (MAEBL), interference lithography (IL), maskless optical-projection lithography (MOPL), zone-plate-array lithography (ZPAL), scanning-probe lithography (SPL), and dip-pen lithography (DPL). We will discuss each briefly and provide some insight into advantages and disadvantages before discussing at length the technique we believe has shown the most promise for solving the current crisis in lithography.

SEBL has been widely used in research for decades and to make masks for the semiconductor industry. The throughput depends on pattern resolution, as shown in Fig. 1, which plots the time required to pattern an area of 1 cm^2 as a function of minimum feature size. For applications in the semiconductor industry, a throughput of ~1 cm^2/s is considered a minimum requirement. Clearly, this requirement is not met for

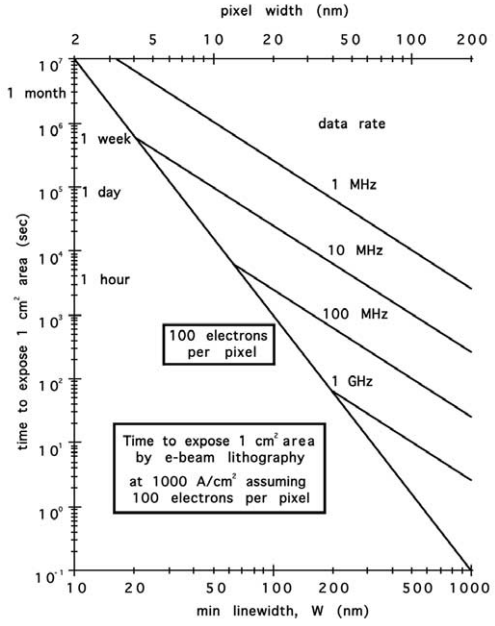

Fig. 1 Plot of the time required to expose a 1 cm^2 area with SEBL as a function of linewidth, assuming that a minimum focal spot or 'pixel' is 1/5 of the linewidth, the current density in the focal spot is 1000 A/cm^2, and shot-noise considerations dictate that at least 100 electrons be incident per pixel. Depending on pixel size, exposure time is determined either by shot noise or the rate at which the beam location is incremented (i.e. the data rate).

linewidths below about 600 nm. MAEBL has been proposed as a solution to this throughput problem[4-7]. However, experimental results with such systems have been limited, and commercial availability is uncertain.

Another problem with SEBL (and with all other forms of electron or ion lithography) is pattern-placement accuracy. Temperature gradients, stray electromagnetic fields, sample charging, vibrations, and a variety of other effects cause the electron beam to deviate from its intended position. Conventional approaches attempt to limit the influence of the disturbances via shielding, temperature control, vibration isolation, and other means, all of which tend to escalate the cost of systems. However, the placement accuracy is seldom better than a few tens of nanometers, which is inadequate in many applications. Another approach to solving the pattern-placement problem is to form a feedback loop that controls the beam position with reference to a fiducial grid on the substrate that has long-range, spatial-phase coherence; a technique called spatial-phase-locked electron-beam lithography (SPLEBL)[8,9]. Placement accuracy approaching 1 nm has been demonstrated[9]. However, SPLEBL is still in the development phase and not yet available commercially. Implementation of spatial-phase locking in multibeam systems has not been attempted.

FIB systems are capable of very high resolution[10] but suffer from worse problems of throughput and placement accuracy than SEBL systems. IL has many forms[11-14] and throughput is quite high. However, it is applicable only to periodic and quasiperiodic patterns, where it excels. SPL[15] and DPL[16] have a number of unique aspects and play an important role in nanostructures research. However, they do not appear to have the general applicability of optical lithography techniques and lack sufficient throughput for applications outside of research. A MOPL system has been proposed that replaces the mask with a programmable micromirror array[17,18]. We discuss this system below in comparison to ZPAL.

Zone-plate-array lithography

In ZPAL, an array of diffractive lenses (e.g. Fresnel zone plates) focuses an array of spots on the surface of a photoresist-coated substrate[19]. The light intensity of each spot is controlled by one element on a spatial light modulator (SLM). The substrate is scanned on a high-precision stage while the elements of the SLM are appropriately controlled, resulting in patterns of arbitrary geometry being written in a 'dot-matrix' fashion. A schematic of ZPAL is shown in Fig. 2.

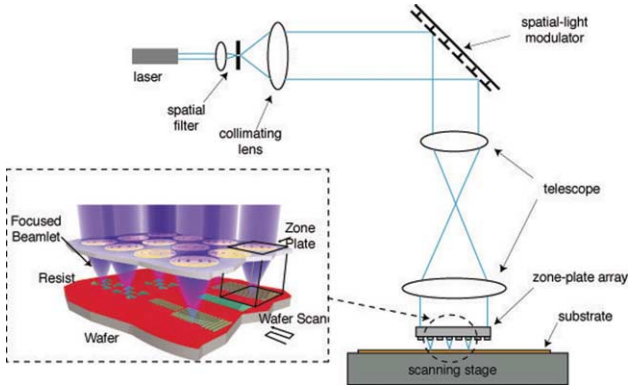

Fig. 2 Schematic of ZPAL. An array of zone plates (diffractive microlenses) focuses normally incident light into an array of spots on the surface of the substrate. Light intensity in each spot is independently controlled by pixels on an upstream SLM. The substrate is scanned and patterns of arbitrary geometry are written in a 'dot-matrix' fashion.

The light source is preferably a continuous wave (CW) laser (a pulsed laser source would severely limit system throughput). Light from the laser is passed through a spatial filter and a collimating lens to create a clean, uniform beam incident on the SLM. The SLM breaks the beam into individually controllable beamlets. A telescope is placed such that each beamlet is normally incident on one zone plate in the array. A Fourier filter within the telescope ensures that there is sufficient contrast between the on and off states. It also prevents cross talk between the beamlets. Each zone plate behaves like a microscopic lens focusing the light into a tight on-axis spot in its focal plane. In the alpha-prototype system at Massachusetts Institute of Technology (MIT)[20], the SLM is a grating light valve (GLV) commercially available from Silicon Light Machines[21].

Alternate zones of the zone plate can either block the transmitted radiation or phase shift it[22]. The former are called 'amplitude zone plates' and the latter 'phase zone plates'. Phase zone plates have much higher focusing efficiency (~40%) than amplitude zone plates (~10%). In the rest of this review, phase zone plates will be assumed, consisting of circular, concentric zones of alternating π and 0 phase shifts. The radii of the zones are chosen such that there is constructive interference at the focus. Fig. 3 shows the working principle of a zone plate and a scanning electron micrograph of the central zones.

The zone-plate array is fabricated using SEBL with a negative electron-beam resist, hydrogen silsesquioxane

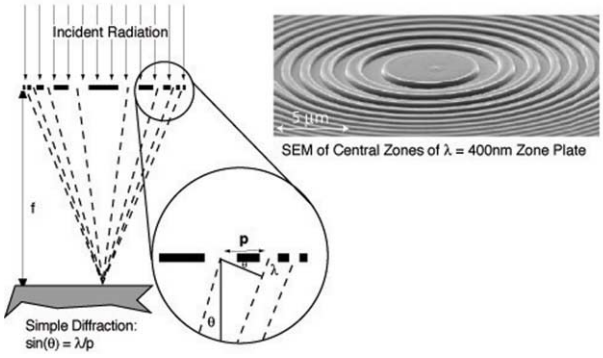

Fig. 3 (Left) Focusing principle of a zone plate. The zones are arranged such that light from adjacent zones interferes constructively at the focus. (Right) Scanning electron micrograph of the central zones of a zone plate.

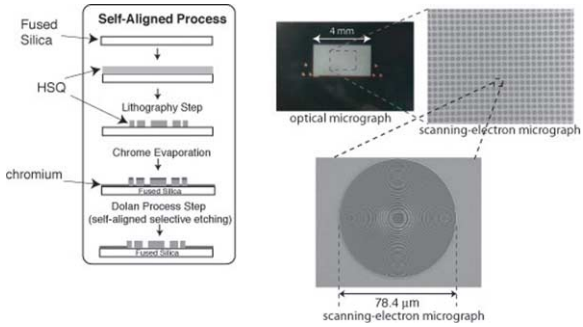

Fig. 4 Zone-plate array fabrication process. The substrate is patterned by SEBL on HSQ. Developed HSQ behaves like fused silica and provides the phase shift for the zone plate. A Fulton-Dolan process[24] is used to define the zone-plate apertures. The final product is shown on the right. Note that the moiré pattern in the magnified image of the zone plate is an artifact of the scanning electron microscopy line scanning.

(HSQ)[23]. After exposure and development, concentric rings of raised HSQ are left on a fused silica substrate. The optical properties of HSQ are close to those of fused silica at ultraviolet (UV) wavelengths. In order to block light transmission in the regions between zone plates, chrome evaporation and self-aligned electrochemical wet etch are performed resulting in self-aligned apertures for the zone plates[23]. The process is illustrated on the left in Fig. 4. On the right, images of an array containing over 1000 zone plates are shown. Since this fabrication process uses robust planar processing techniques, the optical properties of the zone plates are uniform.

Lithographic performance of ZPAL

Patterns of a variety of geometries written using ZPAL are shown in Fig. 5. In Fig. 5a, dense 150 nm lines and spaces are visible. Fig. 5b shows a dense array of holes, part of a photonic band gap device. Fig. 5c is a portion of a concentric ring pattern. An array of elliptical rings, used for studying micromagnetic phenomena[25], is shown in Fig. 5d. Fig. 5e is a ring resonator structure for an integrated optical add/drop filter. Fig. 5f is the ZPAL rendering of the seal of MIT. All the patterns except Fig. 5c were written using a source wavelength, λ, of 400 nm. Fig. 5c was written at λ = 442 nm.

The performance of ZPAL with regard to various lithographic figures-of-merit was evaluated on 150 mm and 200 mm diameter Si wafers. Some of the exposures were performed on an alpha-prototype system at MIT[20] using the GLV SLM and zone plates with a numerical aperture (NA) of 0.7. Others were performed using zone plates of various NAs and a single acousto-optic modulator (AOM). In the latter case, all zone plates wrote the same pattern. All exposures were performed at λ = 400 nm. The substrate wafers were spin coated with 200 nm of BarLi antireflection coating and 200 nm of PFI-88 photoresist. After exposure, the wafers were developed in CD-26 developer for 45 s. Samples were inspected by optical and scanning electron microscopy.

Resolution

The resolution of an optical lithography system is generally expressed by the relationship $W_{min} = k_1(\lambda/NA)$, where W_{min} is the width of the smallest feature, λ is the wavelength, and *NA* is the numerical aperture. The proportionality factor, k_1,

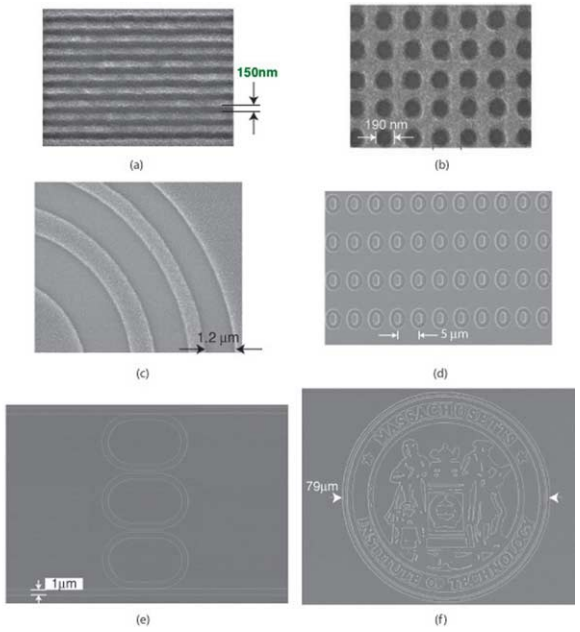

Fig. 5 Scanning electron micrographs of patterns printed in photoresist using phase zone plates.

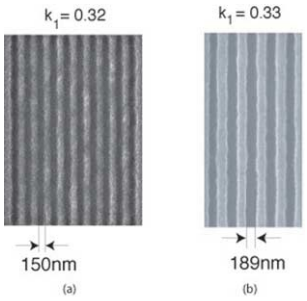

Fig. 6 Resolution in ZPAL. Dense lines and spaces patterned with phase zone plates at λ = 400 nm and (a) NA = 0.85 (using a single AOM) and (b) NA = 0.7 (using the GLV) corresponding to k_1 = 0.32 and 0.33 respectively.

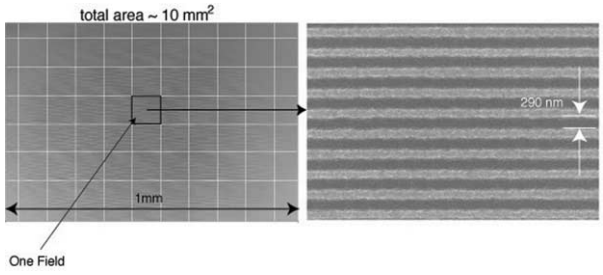

Fig. 7 Scanning electron micrographs of 290 nm lines and spaces covering a ~10 mm² area. Pattern was printed using an array of over 1000 zone plates. Each zone plate wrote an area of 90 mm x 90 mm (a unit cell, depicted as white squares in the image). These patterns were printed using zone plates of NA = 0.7, λ = 400 nm, and a single AOM.

is empirically determined and accounts for process effects. In OPL, as practiced in the semiconductor industry with application of RETs, k_1 values of 0.4 and above are common[26]. Using phase zone plates operating at λ = 400 nm, we have demonstrated[19] k_1 as small as 0.32. In Fig. 6, scanning electron micrographs of dense gratings written using zone plates are shown. The pattern in Fig. 6a was written with zone plates of *NA* = 0.85, whereas that in Fig. 6b was written in our alpha-ZPAL system (*NA* = 0.7)[20]. These results show that ZPAL can achieve at least as good, if not better, resolution than OPL operating at the same wavelength but without resorting to RETs.

The distribution of light in the focal spot of a zone plate (e.g. full width at half maximum of the point-spread function, and height of side lobes) depends on the progression of zones and their phase shift. This can be modified to achieve other than an Airy function distribution[27,28]. Hence, ZPAL provides opportunities for achieving narrower linewidths in much the same way that phase-shift masks achieve this in OPL[29].

Extension to deep-UV wavelengths

Our initial results with zone-plate lithography were obtained with a pulsed ArF laser at 193 nm wavelength[30]. Because it is preferable, for reasons of throughput, to operate ZPAL with a CW source, all subsequent exposures were done with readily available, low-cost CW sources at 442 nm and 400 nm. We believe our results at these wavelengths can be scaled to the deep UV since the HSQ phase-shifting material should perform equally well there. Recently, a CW source at 198 nm wavelength became commercially available. With such a source, dense lines and spaces of 70 nm linewidth should be obtainable without the use of RETs.

It is well known that zone plates work in the X-ray range where they are used for X-ray microscopy[22]. In fact, the first proposal for ZPAL assumed use of 4.5 nm wavelength X-rays from an undulator to achieve 1 cm²/s throughput[31]. Thus, the ZPAL architecture should be extendable to the limits of the lithographic process.

Image contrast

With phase zone plates, only about 40% of the transmitted radiation goes into the focal spot; the remainder forms a background. Hence, it is important to evaluate the extent to which the background radiation degrades the image contrast. This was done by exposing dense lines and spaces over areas that span many unit cells of the zone-plate array. Experiments demonstrated that phase zone plates produce images of sufficient contrast. Fig. 7 shows dense gratings of 290 nm linewidth spanning hundreds of unit cells printed using zone plates of *NA* = 0.7 at λ = 400 nm[19].

Stitching between unit cells

In OPL, a photomask pattern is imaged onto the wafer. In contrast, ZPAL forms an image by printing focused spots in a 'dot-matrix' fashion. There are several modes by which this can be done. The simplest to visualize and analyze, though not the most efficient, is one in which each zone plate in the array is responsible for writing patterns in the unit-cell area of the substrate directly underneath it, which we define as a field. Stitching neighboring fields together forms a final image. The accuracy of stitching across field boundaries is determined primarily by the scanning stage. A secondary factor contributing to stitching error is the placement of zone plates within the array. That placement error can be less than 3 nm (3 σ) if SPLEBL is used in either the global or the segmented-grid mode[8,9].

If the *x*- and *y*-axes of the stage are not collinear with the *x*- and *y*-axes of the zone-plate array, stitching errors will

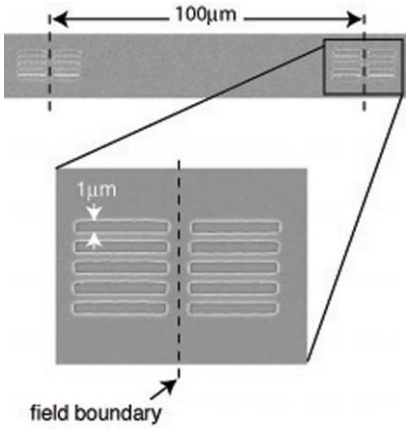

Fig. 8 Scanning electron micrograph of gratings near the field boundaries. Stitching errors across 13 field boundaries were measured and the mean error was estimated as 30 nm.

occur. However, these can be corrected using software. Stitching errors were characterized in the alpha-ZPAL system by measuring the error across all the field boundaries. Using this data as a look-up table, the original pattern was predistorted such that the written pattern was stitched across the fields. Fig. 8 shows scanning electron micrographs of the resulting patterns. The mean stitching error across 13 field boundaries was 30 nm[32], limited by the stage controller, which provides position information through capacitive sensing. A laser-interferometer-controlled scanning stage should achieve stitching errors of less than 5 nm.

For maximum throughput, one would not use the unit cell scanning strategy discussed above. Rather, one would minimize the number of starts and stops by scanning across the full substrate.

Overlay

Another important lithographic figure-of-merit is the alignment of one lithographic step with respect to a previously defined pattern, i.e. overlay. In ZPAL, as in OPL, an external microscope may be used to image alignment marks to achieve overlay. For *in situ* imaging of several alignment marks simultaneously, we developed a simpler technique that uses satellite zone plates as confocal microscopes[33] operating at a nonexposing wavelength (λ = 633 nm). This can achieve fast alignment in x, y, and θ without any external microscopes[32]. Fig. 9a illustrates the technique. The satellite zone plates are located on the periphery of the writing zone-plate array. The position information is fed to the stage controller. Fig. 9b shows a scanning electron micrograph of horizontal gratings printed in two separate lithography steps (labeled level 1 and level 2, respectively). The overlay error measured by the relative shifts between the two gratings was 39 nm in x and 60 nm in y. This was limited by the speed of the system used to capture the images of the alignment marks. We can expect to achieve significantly better alignment using improved hardware. Alternatively, an alignment technique developed originally for proximity lithography, interferometric-spatial-phase imaging (ISPI)[34] could be used. ISPI has demonstrated alignment and overlay ~1 nm.

Proximity-effect correction

In all lithography techniques that involve imaging with photons or charged particles, the width of a printed feature depends on the presence of nearby features. This is referred to as the proximity effect. From a knowledge of the light distribution in the focal spot (i.e. the point-spread function), including the background, one can easily calculate the proximity effects. This is much easier in ZPAL than OPL because there is no coherent relationship between one spot and another, i.e. intensities can be added. By calculating proximity effects before exposure, it is possible to precompensate the exposure dose to correct for these effects. We have developed efficient algorithms to calculate the optimum exposure dose for OPC[35].

The point-spread function can be determined accurately by measuring a large number of single-spot exposures in photoresist and calibrating the measured diameters with the exposure dose. The experimentally measured point-spread function agrees well with a rigorous electromagnetic simulation technique[36]. The rigorous model was used to simulate the proximity effects in a variety of patterns and their optimum exposure dose distributions calculated.

Fig. 10 shows scanning electron micrographs of patterns that illustrate the improvements in pattern fidelity achieved

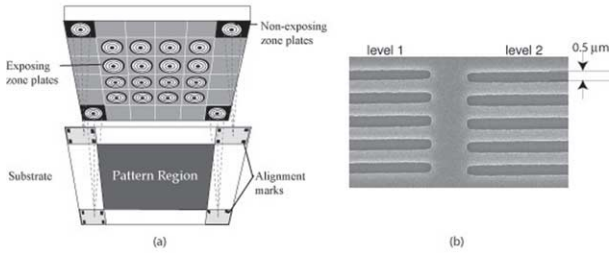

Fig. 9 Overlay in ZPAL. (a) Schematic showing nonexposing satellite zone plates on the periphery of the exposing zone-plate array that are used to image the alignment marks on the substrate in confocal mode. (b) Scanning electron micrograph showing two levels of lithography that were aligned to one another.

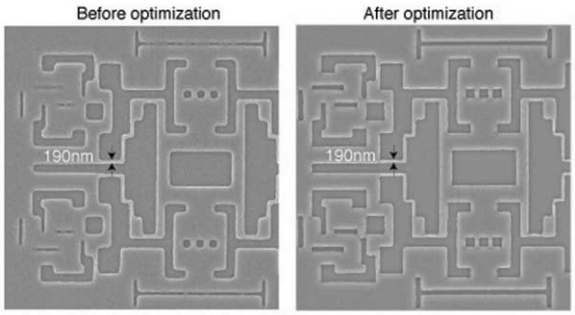

Fig. 10 Scanning electron micrographs of pattern showing improvements from OPC. (Left) Exposure dose was uniform within the pattern. (Right) An optimum exposure dose was used. Patterns were exposed using zone plates at λ = 400 nm, NA = 0.7, and an AOM.

by performing the optimization. The original pattern (Fig. 10, left) received uniform exposure dose throughout, whereas the optimized pattern (Fig. 10, right) received an optimized exposure dose distribution. It was also observed that the optimized pattern was more robust to exposure dose variations, i.e. had higher exposure latitude compared to the original pattern.

This optimization is analogous in its effect to the OPC techniques used in OPL. However, the problem is computationally much simpler with ZPAL because a pattern is formed by an *incoherent* addition of focused spots, i.e. one adds intensities. In OPL the entire image is formed at the same time and hence one must compute the total field created by radiation from all components of a mask pattern and then square that field distribution to obtain the intensity distribution that exposes the resist. This is a much more daunting task and in fact it cannot be solved in closed form; empirical information must supplement the computation.

Throughput

Lithography can be viewed as an information transfer process where the information content on a substrate is proportional to the number of independent pixels per unit area. In OPL, the information stored on a photomask (which amounts to ~10^{11}-10^{12} bits) is transferred onto the substrate in parallel, typically with an exposure time of order 1 s. This high throughput is crucial to the business model of the semiconductor industry. However, the high throughput is achieved at the expense of flexibility and very high cost.

A maskless lithography system such as ZPAL provides flexibility and saves photomask costs at the expense of lower throughput. In ZPAL, the rate of information transfer is the product of the number of zone plates in the array and the switching speed of the SLM. The current SLM has 1088 switching elements and can operate at 0.5 MHz. With that switching speed, 1000 zone plates, and 8 bits per pixels (for 'gray toning'), the information transfer rate is 4 x 10^9 bits/s. The GLV-type SLM can be modified[37] to operate up to ~5 MHz. A SLM of 5000 element illuminating 5000 zone plates, with 8 bits per pixel would result in an information transfer rate of 2 x 10^{11}, or several wafers per hour; about a factor of ten slower than OPL but at least two orders of magnitude faster than SEBL for the same focal spot diameter, as can be seen in Fig. 1. Moreover, with photons, shot noise is orders of magnitude less severe and the particles do not interact. Electrostatic interactions limit the flux in electron-beam systems.

Comparison to maskless optical projection lithography

MOPL in which the photomask is replaced by an SLM consisting of an array of micromirrors is being developed[17,18]. The pattern on the SLM is controlled digitally, and its image is projected onto a wafer by means of a reduction lens.

MOPL utilizes a high-power pulsed laser source whose rate (~kHz) limits the switching speed of the SLM. In order to achieve sufficient throughput, the number of pixels in the SLM has to be inordinately large, e.g. 2048 x 5120 (over ten million). This is a daunting challenge. Since a CW laser source can be used in ZPAL, the smaller number of pixels (and zone plates) is compensated by the much higher switching speed achieved by a fast GLV-based SLM.

In MOPL, several pixels on the SLM are used to print a single pixel in the image on the wafer. This is required to ensure the fidelity of images and to enable the equivalent of phase-shift masks. Since each pixel on a typical SLM is several microns in size, this puts a major burden for demagnification on the refractive optics of the MOPL system. For example, in the commercially proposed system, nine pixels, each of size 8 μm x 8 μm, are used to print one pixel of size 90 nm on the wafer. This requires a demagnification factor of 267, which is higher than any optical microscope lens and probably difficult to achieve with full-image aberration correction. This large demagnification will likely complicate the problem of alignment. The use of refractive optics means that MOPL cannot be extended to wavelengths shorter than 157 nm. In contrast, in ZPAL, the light from one pixel on the SLM is focused to a spot on the substrate by one zone plate. Hence,

the issue of demagnification does not arise. Since zone plates focus on axis without aberration, the resulting image in ZPAL is always aberration free. Moreover, diffractive optics can operate at extreme-UV and X-ray wavelengths.

Analog control of SLM pixels is used in MOPL to achieve sufficient pattern-placement accuracy and pattern fidelity. This requires a transistor and storage capacitor for each pixel in the SLM, which is extremely difficult when the number of pixels is large (around ten million). Furthermore, the response characteristic of each pixel is different and separate correction must be applied to each pixel, increasing the complexity of the system.

In MOPL, one field of the pattern is projected at one time. Then the substrate is scanned before the next field is printed. The stage has to scan the length equivalent to the side of the field, resulting in much larger scan speeds compared to ZPAL, where the stage moves from one spot to another, typically only about 50-100 nm.

Finally, MOPL requires OPC essentially the same as in OPL. Because of the partially coherent nature of the imaging process, the proximity correction is orders of magnitude more difficult to achieve than in ZPAL, where the imaging is completely incoherent (see Fig. 10).

Conclusion

IL and SEBL represent highly effective forms of maskless lithography, especially for research and low-volume, special purpose manufacturing. SEBL can write patterns of arbitrary geometry but suffers from problems of low throughput, high cost, and pattern placement inaccuracy. Two forms of maskless optical lithography have been described, MOPL and ZPAL. The latter has demonstrated the highest quality lithographic results ever reported at 400 nm wavelength and has a clear path to shorter wavelengths, higher resolution, higher throughput, low cost, and commercial availability[38]. ZPAL is an entirely new paradigm that promises to circumvent many of the problems that have troubled OPL and will likely be encountered by MOPL. We believe that ZPAL has the potential to enable low-cost, flexible, high-quality patterning for a wide variety of applications in the field of micro- and nanotechnology. MT

Acknowledgments

The authors would like to thank David Carter, Mark Mondol, Jim Daley, Jim Carter, Fernando Castaño, Euclid Moon, Wonjoon Jung, and George Barbastathis for various contributions to this work. This research was partially funded by DARPA and the Army Research Office under Grant No. DAAD19-01-1-0330.

REFERENCES

1. Valiev, K. A., *The Physics of Submicron Lithography*, Plenum Press, New York, (1992)
2. See, for example, *Proceedings of Annual SPIE Symposia on Microlithography*
3. Owa, S., and Nagasaka, H., *J. Microlitho. Microfab. Microsys.* (2004) **3** (1), 97; Switkes, M., *et al., J. Vac. Sci. Technol. B* (2003) **21** (6), 2794
4. Pease, R. F., Charged Particle Maskless Lithography, Presented at 30th International Conference on Micro & Nano Engineering 2004, to be published *Microelectron. Eng.*
5. Groves, T. R., and Kendall, R. A., *J. Vac. Sci. Technol. B* (1998) **16** (6), 3168
6. Pickard, D. S., *et al., J. Vac. Sci. Technol. B* (2002) **20** (6), 2662
7. Muraki, M., and Gotoh, S., *J. Vac. Sci. Technol. B* (2000) **18** (6), 3061
8. Hastings, J. T., *et al., J. Vac. Sci. Technol. B* (2002) **20** (6), 2753
9. Hastings, J. T., *et al., J. Vac. Sci. Technol. B* (2003) **21** (6), 2650
10. Atkinson, G. M., *et al., J. Vac. Sci. Technol. B* (1992) **10** (6), 3104
11. Walsh, M. E., and Smith, H. I., *J. Vac. Sci. Technol. B* (2001) **19** (6), 2347
12. Savas, T. A., *et al., J. Vac. Sci. Technol. B* (1996) **14** (6), 4167
13. Walsh, M. E., *et al., J. Vac. Sci. Technol. B* (2000) **18** (6), 3539
14. Konkola, P., *et al., J. Vac. Sci. Technol. B* (2003) **21** (6), 3097
15. Kramer, S., *et al., Chem. Rev.* (2003) **103** (11) 4367
16. Ginger, D. S., *et al., Angew. Chem. Int. Ed.* (2003) **43** (11), 30
17. Sandstrom, T., *et al., Proc. SPIE* (2004) **5377** (2), 777
18. Choksi, N., *et al., J. Vac. Sci. Technol. B* (1999) **17** (6), 3047
19. Gil, D., *et al., J. Vac. Sci. Technol. B* (2003) **21** (6), 2810
20. Menon, R., *et al., J. Vac. Sci. Technol. B* (2004), in press
21. Bloom, D. M., *Proc. SPIE* (1997), **3013**, 165
22. Michette, A. G., *Optical Systems for Soft X-rays*, Plenum Press, New York, (1986)
23. Gil, D., *et al., J. Vac. Sci. Technol. B* (2003) **21** (6), 2956
24. Fulton, T. A., and Dolan, G. J., *Appl. Phys. Lett.* (1983) **42** (8) 752
25. Castano, F. J., *et al., J. Vac. Sci. Technol. B* (2004), in press
26. Finders, J., *et al., Proc. SPIE* (2000) **4226**, 1
27. Cao, Q., and Jahns, J., *J. Opt. Soc. Am. A* (2003) **20** (8), 1576
28. Kipp, L., *et al., Nature* (2001) **414**, 184
29. Barbastathis, G., *et al.*, Zone plate array optimization for maskless lithography. To be presented at the 2nd International Conference on Advanced Materials and Nanotechnology, Queenstown, New Zealand, 2005
30. Djomehri, I., *et al., J. Vac. Sci. Technol. B* (1998) **16** (6), 3426
31. Smith, H. I., *J. Vac. Sci. Technol. B* (1996) **14** (6), 4318
32. Menon, R., *et al., J. Vac. Sci. Technol. B* (2004), in press
33. Gil, D., *et al., J. Vac. Sci. Technol. B* (2000) **18** (6), 2881
34. Moon, E., *et al., J. Vac. Sci. Technol. B* (2003) **21** (6), 3112
35. Menon, R., Diffractive Optics for Maskless Lithography and Imaging, PhD dissertation, Massachusetts Institute of Technology, Cambridge, MA, (2003)
36. Prather, D. W., and Shouyuan, S., *J. Opt. Soc. Am. A* (1999) **16** (5), 1131
37. Payne, A., *et al., Proc. SPIE* (2004) **5348**, 76
38. See www.lumarray.com